Citrullination of Fibronectin alters integrin clustering and focal adhesion stability promoting stromal cell invasion

Victoria L. Stefanelli[1,2], Shilpa Choudhury[1], Ping Hu[3], Yining Liu[4], Anja Schwnenzer[5], Vincent Yeh[3], Dwight M. Chambers[1,2], Kelly Pesson[1], Wei Li[1,3], Tatiana Segura[4], Kim S. Midwood[5], Matthew Torres[1], Thomas H. Barker[3*]

[1]Georgia Institute of Technology, Atlanta, GA, USA; [2]Emory University, Atlanta GA, USA; [3]University of Virginia, Charlottesville, VA USA; [4]Duke University, Durham, NC, USA; [5]University of Oxford, Oxford UK

Abstract

The extracellular matrix (ECM) microenvironment is increasingly implicated in the instruction of pathologically relevant cell behaviors, from aberrant transdifferentation to invasion and beyond. Indeed, pathologic ECMs possess a panoply of alterations that provide deleterious instructions to resident cells. Here we demonstrate the precise manner in which the ECM protein fibronectin (FN) undergoes the posttranslational modification citrullination in response to peptidyl-arginine deiminase (PAD), an enzyme associated with innate immune cell activity and implicated in systemic ECM-centric diseases, like cancer, fibrosis and rheumatoid arthritis. FN can be citrullinated in at least 24 locations, 5 of which reside in FN's primary cell-binding domain. Citrullination of FN alters integrin clustering, focal adhesion stability and concomitant enhancement in force-triggered integrin signaling along the FAK-Src and ILK-Parvin pathways within fibroblasts. In vitro migration and in vivo wound healing studies demonstrate the ability of citrullinated FN to support a more migratory/invasive phenotype that enables more rapid wound closure. These findings highlight the potential of ECM, particularly FN, to "record" inflammatory insults via post-translational modification by inflammation-associated enzymes that are subsequently "read" by resident tissue fibroblasts, establishing a direct link between inflammation and tissue homeostasis and pathogenesis through the matrix.

Keywords:
Citrullination, Fibronectin, Fibroblast, Integrins, Mechanotransduction, Cell Migration

Introduction:

The provisional extracellular matrix (ECM) is a veritable wellspring of biological cues—both biochemical and biophysical—that serves to instruct cell phenotypes [1]. In pathologic conditions, and especially in the cases of cancer and fibrosis, the ECM is known to acquire substantial changes [2, 3] in composition, structure, and mechanics, which together exacerbate disease etiology through promotion of angiogenesis [4], cell differentiation [5, 6], and immune activation [7], among other events.

One often overlooked source of pathologic ECM modification is citrullination, a posttranslational modification (PTM) that converts certain arginine residues into citrulline and which is exclusively catalyzed by a class of enzymes called peptidyl arginine deiminases (PADs) [8-11]. Citrullination is tightly associated with inflammation due to a combination of PADs being predominately expressed and secreted by macrophages and neutrophils, but also the fact that they require supraphysiological calcium concentrations for activation [12, 13]. Thus, citrullination tends to be extensively present in a variety of chronic inflammatory conditions, especially rheumatoid arthritis (RA)[9], malignant cancers [14, 15], and lung fibrosis [16].

It's well-established that citrullinated proteins can potentiate an autoimmune response, most notably in the form of anti-citrullinated peptide antibodies (ACPA), which can be detected up to about 10 years prior to RA onset [17]. ACPA titer correlates with disease severity, and its detection is currently considered the gold standard in RA diagnosis [18, 19]. Beyond an antibody response, citrullinated proteins are capable of

Abbreviations:
FN- Fibronectin
CitFN- Citrullinated Fibronectin
PAD- Peptidyl Arginine Deiminase

stimulating the immune system through enhancement of cytokine secretion in T cells [20] and macrophages [21], promotion of T cell proliferation [20], and binding to major histocompatibility complex (MHC) molecules with greater affinity [22] than their non-citrullinated counterparts due to a positive charge in the P4 pocket of the HLA-DR shared epitope (SE) combined with elimination of positive charge that occurs with citrullination [23] .

There is, however, currently a dearth of research on the impact of citrullinated ECM on non-immune cell types, including mesenchymal stromal cells such as fibroblasts, considered to be central drivers of multiple diseases including fibrosis, cancer, and RA. This fundamental gap in our understanding is especially striking when considering citrullination's relatively long-lived presence in the cellular microenvironment since it is an irreversible modification [8] that renders many ECM proteins resistant to degradation [24].

Therefore, in the current study, we first investigate the potential extent of citrullination of the provisional/wound repair ECM protein FN by the key inflammation-associated PADs. We further characterize the impact of FN citrullination on its ability to coordinate integrin interaction, trigger normal downstream signaling, and influence fibroblast function relevant to inflammatory pathologies. Our results highlight citrullinated fibronectin (cFN) as a modifier of integrin-FN clustering dynamics, mechanotransductive signaling leading to mimicry of wound healing phenotypes in fibroblasts even in the absence of additional inflammatory cues, suggesting that inflammation may act to prime the ECM to support subsequent fibroblast activation.

Results:

Identification of 24 enzyme-specific citrullination sites in fibronectin via mass spectrometry

To determine the full range of potential citrullination sites within FN, we used a combination of proteolytic enzymes and LC-MS (see methods) on plasma-purified human FN modified *in vitro* by PAD2 alone, PAD4 alone, or PADs 2 and 4 together. Citrullination was confirmed was verified by SDS-PAGE, COLDER assay and Dot Blot (Supplementary Fig. 1). We specifically chose to analyze PAD isotypes 2 and 4 because they are known to be the main actors in cancer [14, 15], RA [9], and fibrotic diseases [16, 25]. MS analysis identified 24 unique citrullination sites across an aggregate protein coverage of 81% percent (Fig. 1A; Supplementary File 1; Supplementary Fig. 2), including 3 previously reported sites (R1035, R1036, and R2356)[26, 27]. A majority of these sites (14 total) reside within FN regions possessing known physiological functions including that of fibrin, collagen, and heparin binding (Supplementary Fig. 3A). A complete table containing all details regarding the MS analysis is provided (Supplementary File 1)

Five citrullination sites were identified within the primary cell-binding domain of FN (the 9^{th} and 10^{th} type III repeats of FN, $^{9\text{-}10}$FN-III), three of which (R1479, R1476, R1452) were located near the canonical integrin binding tripeptide motif RGD on the 10^{th} type III repeat (Fig. 1B). This simple motif is capable of binding about half of all known integrins, including αvβ3 and α5β1. The RGD site itself was unmodified, in agreement with previous MS analyses of cFN from RA patient samples [26]. However, we did observe citrullination at R1434 and R1410, both within the adjacent 9^{th} type III repeat (Fig 1B). R1410, aka the synergy site, is part of the pentapeptide motif (PHSRN) and is critical for strengthening α5β1 integrin and implicated in α3β1and α4β1 integrin attachment in coordination with RGD [28]. Previous studies have highlighted the conformation sensitivity of $^{9\text{-}10}$FN-III in regulating integrin selectivity and binding affinity [29], and thus any of these five sites potentially influences the affinity of the dominant fibroblast integrins, αvβ3 and α5β1.

As expected, citrullination was specific in varying degrees to the enzymatic activity of individual PADs as estimated by a comparison of peptide spectral matches (PSMs) across all experiments (Supplementary Figs. 3B, 4). Only 10 FN citrullination sites—less than half those identified—were found to be modified by both PADs 2 and 4. These enzymes displayed distinct preferences for amino acid sequence, with PAD4 exhibiting an overall more aggressive modification profile with six unique modifications compared to only four unique modifications attributed to PAD2. Of potential biological importance is the fact that the PHSRN synergy site (R1410) was modified exclusively by PAD2, the iso-enzyme possessing the distinct capability of being secreted by non-activated neutrophils [13]. This indicates that PAD2 may be of greater importance in the context of altering physiological function during tissue remodeling.

Citrullination of fibronectin alters integrin clustering.

To determine whether αvβ3 or α5β1 attachment to FN as a membrane-bound cell receptor is functionally impacted by citrullination, CHO-B2 cells which do not express integrin (a kind gift from Martin Humphries) transfected with αv and β3 express vectors (CHO-B2.αvβ3) or CHO-K1 cells (intrinsically expressing only α5β1) were challenged in binding to FN, fibrinogen (Fib), or their citrullinated counterparts in an adhesion assay. Citrullination of FN resulted in a reduction of the number of adhered CHO-B2.αvβ3 cells by about half, whereas citrullination of fibrinogen (which support αvβ3 attachment mainly through an RGD motif) resulted in elimination of CHO-B2.αvβ3 cell adhesion (Supplemental Fig. 5A). No differences were observed in CHO-K1 adhesion to cFN compared to FN (Supplemental Fig. 5B).

Native stromal cells possess at least six FN-binding integrin heterodimers [30] with well-documented abilities to cooperatively bind, cluster, and/or compensate for one another in the formation of focal adhesions (FAs)[31, 32]. We therefore visualized integrins within FAs of human foreskin fibroblasts (HFF) by immunofluorescence (IF) to investigate integrin preference on FN and cFN (Fig. 2A, B). No statistically significant changes in αv or αvβ3 signal within FA complexes (as identified by paxillin) were observed (Fig. 2C), while several α5β1-linked enhancements were noted on cFN compared to FN. The quantity of α5 and β1 subunits (determined by signal intensity) within FA complexes was elevated on cFN (Fig. 2C). As visually observed in ratiometric images of integrins within focal adhesions (Fig. 2A, B) and quantitation (Fig. 2D) the ratios of β1 and α5 compared to αvβ3 within FAs demonstrates significantly elevated β1:αvβ3 and α5:αvβ3 in cells seeded on cFN compared to FN. Finally, the pairwise co-localization of integrin subtypes was elevated on cFN, regardless of the integrins being compared (Fig. 2E). This latter finding points towards an enhancement of integrin clustering on cFN compared to FN. Similar findings were noted on human lung fibroblasts (Supplementary Fig. 5C). cFN also supported slightly greater clustering of αv and α5 independent of force application to FAs (Supplementary Fig 5D).

When β1 integrins were knocked down by shRNA, a reduction in clustering is observed (Supplementary Fig. 5F) as well as a decrease in the average FA size on both FN and cFN, though to a greater extent on cFN (Supplementary Fig 5G). These data suggest cFN has a stronger dependency on β1 integrin clustering which then facilitates co-clustering of αvβ3. This is additionally evidenced by the fact that αvβ3 presence within FAs of β1 knockdown fibroblasts significantly decreases on cFN but not FN (Supplementary Fig. 5F), suggesting integrin cooperativity; there is a strong reliance of αvβ3 recruitment on α5β1 integrin engagement of cFN. These data suggest that fibroblasts experience a fairly dramatic switch in the dynamics of integrin binding during FA formation in response to FN citrullination. On native unmodified FN, it has been shown that rapid αvβ3 association takes place first and leads to subsequent α5β1 co-recruitment into FAs [33]. This order/dependency is reversed on cFN.

Citrullination of fibronectin alters the cytoskeletal/contractile activity of stromal cells

One indicator of integrin signaling and proper mechanotransduction is “compliance matching”. The bulk Young’s modulus of a properly signaling cell, especially fibroblasts, is linearly proportional to its underlying matrix stiffness up to ~10-12kPa (cell stiffness ~ 5-6 kPa). Therefore, we performed single-cell atomic force microscopy (AFM) to probe the stiffness of HFFs plated on FN or cFN coated glass coverslips (~3 GPa stiffness). Fibroblasts adhere less well on cFN coated glass and are significantly smaller and more round by observation (Figure 3B, D, Supplementary Fig. 6), yet they display a similar or higher bulk modulus (5.773 kPa) than fibroblasts on FN (4.536 kPa; Fig. 3A). This enhanced cell stiffness (suggestive of elevated cortical actin assembly) despite being less well spread on cFN versus FN was also observed when HFFs were plated on 9 kPa “soft” polyacrylamide gels (Supplementary Fig. 5E).

Assembly of intracellular actin fibers is also coincident with fibroblast compliance matching and normal integrin signaling and mechanotransduction. Fibroblasts will form these on substrates starting around 3kPa, with progressive amounts of bundling into actin stress fibers with increasing stiffness [34, 35]. Indeed, we demonstrate enhanced actin content within HFFs on cFN (Fig. 3C) that appears to exhibit some level of

substrate stiffness dependence (Supplementary Fig. 7D, E). Enhanced actin polymerization and bundling on cFN may contribute, in part, to the aforementioned enhanced bulk moduli observed on cFN. To further assess the contractile phenotype of fibroblasts on cFN versus FN we performed traction force microscopy. Defined patterns of cFN and FN stamped onto soft polyacrylamide gels act both as anchoring points for FAs and fiduciary markers to analyze cell-derived forces. HFFs plated and spread on cFN display significantly less contractile forces than HFFs on FN. Thus HFFs on cFN are smaller and less contractile, yet display a high level of polymerized actin, suggesting differences in FA signaling and normal force-mediated feedback loops that help to establish mechanical homeostasis between a cell and its microenvironment.

To directly probe signaling associated with individual FAs in the presence or absence of force, we performed force-inducible immunoprecipitation (force-IP or f-IP) experiments (Fig. 4A), which pointedly bypasses the artificially imposed "tensioned" state achieved by cells on glass due to stiffness matching. Here, we observed greater baseline (i.e. no force, clustering-associated) activation states of FAK, Src, and ILK in FAs engaging cFN compared to FN (Fig. 4B, Supplementary Fig. 7C), with substantial further enhancement upon force stimulation. These findings were most striking in the case of ILK. They were confirmed with standard IF analysis of FA-associated, active (i.e. phospho-) FAK(Y397) and Src, along with vinculin, which revealed significant elevation in each their quantity (Fig. 4C) and co-localization within FAs (Fig. 4D) on cFN compared to FN. Active cellular ILK was likewise significantly increased on cFN surfaces (Fig. 4E). GLISA analysis of Rac and Rho signaling did not reveal any differences (Supplementary Fig. 7A, B). Nevertheless, confocal z-stack analysis of a central downstream ILK target, glycogen synthase kinase (GSK) revealed a significant enhancement on cFN compared FN (Fig. 4F-H). We interpret these data as suggesting cFN exposure leads to heightened activation of both the FAK-Src and kindlin-ILK-GSK signaling axes.

Enhancement of focal adhesion turnover and fibroblast cell migration

Elevated levels of both pFAK and pGSK have been previously associated with elevated FA turnover and cell migration [36, 37]. This fact, along with our observation that HFFs engaging cFN generate smaller contractile forces, led us to directly explored cFN's influence on FA stability and turnover. Immunofluorescent staining for α-actinin, a proxy marker for stable FAs, illustrates significant reductions in α-actinin signal intensity within FAs (Fig. 5A, C), α-actinin positive FAs (i.e. Mander's coefficient; Fig. 5B), and Pearson's correlation coefficient (r) between paxillin and α-actinin stain on cFN compared to FN (Supplementary Fig. 8A). These data strongly suggest that HFF FAs are less stable on cFN compared to unmodified FN. Knockdown of β1 integrins reversed this trend, suggesting that differences in FA stability are, at least in part, mediated through β1integrin signaling. As expected, both FAK inhibition (PF-28) and F-actin destabilization (cytochalasin D) reversed this trend to an even greater extent than β1 knockdown.

Analysis of TIRF videos of HFFs transfected with RFP-paxillin on FN or cFN revealed shorter FA lifetime on cFN compared to FN with average lifetimes of 196.5 seconds compared to 229.2 respectively, out of a maximum of 600 seconds (Fig. 5D). Histograms of FA lifetimes suggest a trend of elevated populations of very short-lived FAs on cFN concurrent with long-duration FAs on FN (Supplementary Fig. 8B). The rate of displacement of FAs on cFN (0.0187 um/sec) was elevated compared to FN (0.01247um/sec, Fig 5E).

Enhanced focal adhesion turn over and less contractile force generation strongly suggest a migratory, non-contractile phenotype. Random cell migration was investigated through time-lapse microscopy. HFFs possess greater average velocities (Fig. 5F, Supplementary Fig 8C) on cFN substrates (0.1887 um/min) compared to FN (0.1606 um/min) and enhanced persistence on cFN compared to FN (Fig. 5G,H; Supplementary Fig. 8D). *In vitro* wound healing assays reveal greater overall wound coverage by HFFs on cFN surfaces compared to FN (Fig 5I, J). These results together suggest that cFN can promote a more invasive fibroblast phenotype.

To confirm that this phenotype holds true on a softer, more physiological matrix, gel contraction assays utilizing 3D fibrin/FN gels that were completely citrullinated, or not, were conducted. In both strained (Supplementary Fig. 8E, F) and floating versions of this assay, HFFs on the citrullinated gel constructs possessed a diminished capacity to contract the gels, (a finding typical in highly migratory cell types [38]). Fast FA turnover in invasive cells leads to repeated release of tension between the cell and its ECM, thus inhibiting gel contraction [39]. These data suggest that even in soft 3D ECM, HFFs display enhanced migratory capacity in response to cFN, compared to FN.

Citrullinated fibronectin/fragment shows a trend for accelerating wound closure and increasing cell infiltration

Based on the results from our *in vitro* study, we hypothesized that with enhanced fibroblast/stromal cell migration, citrullination of FN and possibly $^{9\text{-}10}$FN-III might accelerate wound closure and increase cell infiltration. Two experiments were performed comparing FN with cFN and the integrin binding domain of FN ($^{9\text{-}10}$FN-III) also with and without citrulline modification. Although the overall wound closure rate, granulation tissue, and collagen deposition were similar among all conditions, differences in gross wound closure rates revealed that cFN treated wounds healed significantly faster than the FN group (Figure 6). Further, quantification of cell nuclei in the wound bed revealed that the c$^{9\text{-}10}$FN-III treated wounds had significantly higher cell nuclei present compared to the $^{9\text{-}10}$FN-III control (Supplementary Fig. 9). These *in vivo* wound healing studies, although limited, suggest elevated cellular invasion and would closure in the presence of cFN compared to FN.

cFN1410 is a citrullinated epitope recognized by antibodies in rheumatoid arthritis patients

Citrullinated peptides can provoke an ~~As discussed previously, the~~ autoantibody response in patients with rheumatoid arthritis (RA)~~ can be directed against citrullinated peptides~~, and anti-citrullinated peptide antibodies (ACPA) are well established markers for diagnosing the disease [40, 41].

Therefore, ~~Based on our *in vitro* and *in vivo* studies,~~ we designed four FN peptides across the integrin binding $^{9\text{-}10}$FN-III encompassing citrulline residues that were identified by mass spectrometry, and their corresponding arginine-containing control peptides (see Supplementary Table 1), and~~were used to~~ analyzed antibody responses in RA patients (n=22) and healthy controls (n=23) by ELISA. Antibodies recognizing citrullinated FN peptide cFN1410 (CIT in Figure 7) were detected in serum samples from 55% of patients, but not in control sera, and no significant response against the arginine control peptide (ARG) was observed (Figure 7A). Furthermore, there was no correlation between antibody responses towards the cFN1410 and FN1410 peptide in RA sera ($r=0.2776$, $p=0.2109$) (Figure 7B), confirming that antibody responses towards cFN1410 are citrulline-specific. No citrulline specific response to any other peptide tested from fibronectin was detected (Supplementary Figure 10).

Discussion:

The established ability of integrin αvβ3 to bind and unbind more quickly is what many believe allows this integrin to mediate mechanotransduction and distinguish variations in stiffness and stretch more dramatically than α5β1 at low substrate stiffnesses [33, 42]. Nevertheless, α5β1 integrins also respond to changes in substrate stiffness, and they have been suggested to possess an even greater role than αvβ3 in mechanotransduction on higher stiffness substrates and in the presence of force [43-45]. The strength of α5β1 attachment is greater than that of either αv integrins alone or that of αv and β1 integrins together [33]. Integrin α5β1 engaging ECM exists in both relaxed (binding only to RGD) or tensioned (binding to RGD + PHSRN) states, the latter of which is ~100 times stronger than that of the former [28, 46]. Importantly, the ratio of α5β1 integrins in the tensioned state correlates both with applied shear stress and substrate stiffness [46]. Therefore, it is likely that α5β1 integrins employ changes in state as a mechanism of force sensing in both stiff and high-stress environments.

Herein we report that citrullination of the ECM protein FN appears to result in a shift in integrin binding preference in stromal cells from αvβ3 to α5β1 possibly through both diminished αvβ3 affinity and altered α5β1 adhesion, though we do not directly explore the specifics of integrin binding dynamics in this work. Our interpretations are based on a biologically meaningful decrease in attachment of CHO-B2.αvβ3 cells to cFN and the dependency of αvβ3 clustering in FA engaging cFN on β1 integrin expression. Mechanistically, reduction in αvβ3 affinity could provide the traditionally slower-binding α5β1 integrin a competitive advantage, as evident through enhanced α5 and β1 fluorescent signals within FAs engaging cFN. This is especially evident at early time points, where citrullination causes a decrease in overall stromal cell adhesion, a characteristic confirmed by others [47].

The precise molecular mechanism underlying this potential integrin shift is as of yet unclear. Of the five FN citrullination sites identified within the cell-binding domain, only one (R1410) reacted significantly with RA patient serum, suggesting a relevant frequency in these patients. Electron microscopy analysis of α5β1 engaging with PHSRN has shown that the two entities do not make physical contact [48], and thus it is not obvious how citrullination at this location would act to strengthen α5β1 attachments. $^{9\text{-}10}$FN-III is also notoriously conformation sensitive, and thus it is possible that citrullination at R1434, 1452, 1476, and/or 1469 may function to enhance or reduce α5β1/ αvβ3 attachment, respectively. While screening of these citrullination sites with RA serum did not produce significant differences, it should be acknowledged that citrullinated proteins found in RA synovial fluid far outnumber those that are known to produce an ACPA response; i.e. a unique ACPA does not exist for every citrullination site in RA patients[49]. Thus, our inability to positively identify ACPAs to these specific sites in RA serum does not conclusively deny their *in vivo* presence. Site-specific mutagenesis of each citrullination site followed by interferometry and/or functional cellular assays would be required, but not likely sufficient, to definitively pinpoint the relative importance of individual citrullination sites, though this would be an interesting area for future study.

Our working hypothesis is that citrullination artificially forces fibroblasts into an attachment state somewhat skewed in favor of α5β1 integrins and that effectively mimics high-stress (tensioned) states. This hypothesis is supported by fIP results that demonstrate FAs engaging cFN are more sensitive then FN-engaged FAs, i.e. display more robust signaling, in response to an identical force. However, how these altered extrinsic cues are interpreted, phenotypically, is not completely clear. AFM results that imply the cells are interpreting their substrates as being artificially stiffer. Enhanced integrin clustering corroborates this result; stiffer substrates promote more integrin clustering [35]. Furthermore, tensioned α5β1 leads to phosphorylation of FAK at Y397 [46], an event observed in this study. Phospho-FAK was enhanced on cFN compared to FN in the presence of force, implying that citrullination of FN may prime cells for a more robust force-induced signaling. Yet, fibroblasts on cFN also display far less contractile force, as demonstrated in TFM experiments. This result may be due to the inherent mechanical homeostasis exhibited in FAs. If FAs are hypersensitive to forces, such as in the case of cFN-engaged FAs, they may reach tensional homeostasis at far lower forces than normal.

cFN-mediated signaling appears to activate both the FAK-SRC and Kindlin-Pinch-ILK signaling axes. Phospho-FAK is essential to FA turnover [50] and its inhibition is known to reduce fibroblast migration [51]. Phospho-ILK acts as a scaffolding protein with Pinch and Parvin and as an independent kinase. The ILK-parvin axis promotes vinculin recruitment and F-actin stabilization, downstream phenomenon directly observed in our study. ILK phosphorylation of GSK at Ser9, as observed here, renders it inactive and unable to sequester β-catenin, among other targets, thus promoting activation of the canonical β-catenin/WNT signaling pathway [36] that drives differentiation, survival, and invasiveness. Thus, the signaling observed in response to fibroblast engagement of cFN strongly supports the enhanced focal adhesion turnover and migratory behavior we document. Anecdotally, pharmacological GSK inhibition has been associated with myofibroblast differentiation and fibrotic exacerbations [52].

It should be noted that the results reported here were obtained in mostly 2D environments pointedly controlled such that cFN constituted the single differentiating experimental factor. Practically speaking, this is an overly simplified representation of an *in vivo* cell microenvironment. Stromal cell interactions are known to be substantially altered in 3D environments such that α5 integrins play an even more dominant role in adhesion, proliferation, migration, and spindle morphology [43]. Furthermore, in an inflammatory environment, cells are exposed to a multitude of soluble stimuli including cytokines and growth factors that alter or accentuate various phenotypes. For example, activated synovial fibroblasts isolated from human RA patients exhibit enhanced cytokine secretion and apoptotic resistance when subsequently exposed to cFN *in vitro* [53], the latter of which we were unable to replicate using healthy fibroblasts. Thus, in an *in vivo* environment replete with inflammatory stimuli, such as that tested in our *in vivo* dermal wound healing assay, cFN likely influences not only cell migration but also several additional phenotypes. On the contrary, cFN would be one of many extrinsic cues, thus its impact on tissue repair/remodeling processes complicated.

Our results are especially unique in their depiction of citrullinated ECM as an activating influence on stromal cells. Previous investigations of collagen II [26, 54], collagen IX [54], fibrinogen [26], and even FN [26, 47] (with non-modified PHSRN) suggest that citrullination promotes fibroblast senescence. Given the significance of fibroblast-FN interactions during embryogenesis [55], it is enticing to suggest a possible

evolutionarily-conserved, innate function of cFN activation of stromal cells in tissue remodeling and wound healing, which in excess promotes aberrant wound healing phenotypes characteristic of fibrotic and malignant pathologies. Indeed, certain cancer cells are completely dependent on α5β1 for attachment to FN [56], and overexpression of α5β1 integrin in lung carcinomas is associated with increased tumor growth and malignancy [57]. Citrullination-induced α5β1 enhancement may therefore constitute an intermediate malignant state.

Citrullination is a pervasive phenomenon tightly associated with a range of chronic inflammatory conditions, and outside of degradation, it seems to exist as an insidious cue to which cells can respond long after the initiating inflammatory event has subdued—i.e. it constitutes a means for recording inflammatory memories within the ECM. It therefore represents an important additional consideration in not only disease progression but in the use of decellularized tissues for regenerative medicine endeavors. Efforts are under way to develop anti-citrullination therapies, many of which have already shown promise in pre-clinical models for atherosclerosis [58], RA [59], lupus [60], multiple sclerosis [61], inflammatory colitis [62], and colorectal cancer [63]. Evidence for both immune and now fibroblast cell activation through citrullinated ECM molecules point towards a need to better understand the role this PTM plays in directing disease-relevant cell phenotypes.

Methods:

Protein Citrullination:

Unless otherwise mentioned, all proteins were citrullinated as follows, in a PAD reaction buffer containing final concentrations of 100mM Tris-HCl, 5mM $CaCl_2$, 0.3mg/mL protein and at pH 7.4. Proteins were incubated with 10U/mL PAD4 (Cayman Chemical) and 5.6μg/mL PAD2 (SignalChem) at room temperature overnight with shaking at 200 rpm after which reactions were quenched with 20mM EDTA. In all cases, non-citrullined proteins used for experimental comparisons were subjected to identical buffers and incubation conditions with the exception of PAD enzyme presence.

Cell Culture:

Unless otherwise specified, all experiments utilized Human Foreskin Fibroblasts (HFFs) from ATCC at or below passage twelve and maintained according to ATCC recommendations. All experiments were performed in standard media without serum, designated serum-free media, or SFM, unless otherwise specified. Quenching of trypsin reactions prior to plating in SFM was carried out with soybean trypsin inhibitor (Sigma). For some longer-duration experiments, SFM was Supplemented with a small amount of FBS from which fibronectin (FN) had previously been depleted. Knockdown of β1 integrin was carried out using β1 shRNA plasmids (sc-72028-SH) and β1 lentiviral particles (sc-72028-V), or control shRNA lentiviral particles (sc-108080) from Santa Cruz.

Citrullination Verification:

A combination of SDS PAGE (Supplementary Fig. 1A), dot blots using anti-peptidyl citrulline antibody (Millipore MABN328) at 1:4000 (Supplementary Fig. 1C), and the COLDER assay as described by Knipp. et. al. [64] were utilized to both titrate PADs 2 and 4 (Supplementary Fig. 1B) as well as to verify modification of individual batches of protein.

Preparation of Substrates:

Unless otherwise mentioned, all surfaces were coated with proteins by incubating the protein of choice in PBS at a concentration of 20μg/mL overnight at 4ºC, followed by blocking in 1% heat-denatured bovine serum albumin (sigma aldrich) 30 minutes. All FN was isolated in-house from fresh human plasma using gelatin-sepharose beads with confirmation of purity via gel electrophoresis and coomasie stain. All fibrinogen utilized was FIB3 from Enzyme Research Labs.

In-Gel Protein Digestion for Mass Spectrometry:

In-gel protein digestion was conducted as previously described [65], with modifications. Briefly, selected protein bands were excised from the Coomassie-stained gel, diced into small pieces, and then de-stained with HPLC-grade water (Avantor) and 1:1 acetonitrile (ACN)/ammonium bicarbonate (ABC) (Sigma-Aldrich). De-

stained gel pieces were dehydrated with multiple ACN washes until rock hard, followed by air drying for 10 minutes. Gel pieces were rehydrated for 30 minutes with 50mM dithiothreitol (Sigma-Aldrich), followed by replacement with 100mM iodoacetic acid (Sigma-Aldrich) and 45 minutes shaking at 750 rpm in the dark to alkylate the reduced thiols. After reduction/alkylation, the gel pieces were once again washed and dehydrated as before, and then chilled on ice for 10 minutes. In-gel digestion was achieved by rehydrating the gel pieces with either trypsin (40µg/mL, Promega Cat # V511A), gluC (40µg/mL, Calbiochem Cat # 324713), chymotrypsin (50µg/mL, Promega Cat # V1062), or a mixture of trypsin and gluC. In each case, 50µL of the sequencing grade enzyme solution was added to the gel pieces and incubated on ice for 30 minutes. Excess enzyme solution was then removed and replaced with 50mM ABC, and the pieces were incubated overnight at 37°C with shaking at 750 rpm. Resultant proteolytic peptides were extracted by two rounds of dehydration using ACN and collection of the resulting extract into low-retention microfuge tubes, which were frozen solid at -80°C and then sublimated by centri-vapping. The dried peptides were reconstituted by sonication in 5% ACN/0.1% formic acid and stored at -80°C prior to analysis.

Mass Spectrometry:

LC-MS analysis of fibronectin peptides produced by in-gel digestion was carried out with an UltiMate™ 3000 RSLCnano System UPLC system (Dionex) with Acclaim PepMap RSLC column (75µm x 25cm nanoViper C18 2µm, 100Å) coupled to a Q-Exactive Plus Orbitrap mass spectrometer (Thermo Scientific) run in data-dependent acquisition mode. Resultant RAW files were analyzed using Proteome Discoverer 2.1 with embedded SEQUEST search algorithm operating with an allowable 1% false-discovery rate, wherein the human fibronectin (P02751) isoforms 1-17 were used as targets for spectral matching. Mass deviations for precursor ions and fragment ions were set to 10 ppm and 0.6 Da respectively. Besides citrullination (R), other modifications such as deamidation (N, Q), oxidation (M), phosphorylation (S, T, Y), acetylation (protein N-terminus), and caramidomethylation (C) were included in the analysis. Additionally, all MS/MS spectra revealing citrullinated sites were checked manually.

CHO Cell Adhesion Assays

CHO-K1 and CHO-B2 cells transfected with αvβ3 were plated on FN- or cFN-coated (and blocked with heat-denatured Bovine Serum Albumin (hdBSA) coverslips for 1 hour at a density of 5000cells/cm^2. As a negative control, CHO-αvβ3 cells were also plated on coverslips coated with fibrinogen or citrullinated fibrinogen. Cells were subsequently washed with PBS++ (supplemented with 2mM Ca^{2+} and 1mM mg^{2+} for maintenance of integrin activation), fixed with 4% paraformaldehyde, and stained with fluorescent phalloidin and hoescht. Fluorescent microscopy was utilized to determine the number of cells remaining attached post-washing.

Immunocytochemistry Staining:

HFFs were plated on FN/cFN or poly-L-lysine (PLL)-coated coverslips at 5000 cells/cm^2 for 30 minutes at which point they were washed 1X with PBS++ (2mM $CaCl_2$, 1mM $MgCl_2$), fixed with 4% paraformaldehyde, permeablized with 0.2% triton-X, blocked with normal goat serum and incubated with primary antibody sets, as appropriate, overnight at 4ºC. The following primary antibodies were used: anti-β1 (9EG7) at 1:500, anti- αvβ3 (LM609) at 1:200, anti-α5 (AB1928) at 1:500, anti-alpha V (272-17E6, abcam16821), rabbit anti-paxillin (Y113, ab32084, Abcam) at 1:400, mouse anti-paxillin (ThermoFischer SH11) at 1:300, anti-GSK (Cell Signaling mAb #9832) at 1:250, anti-phospho-s9 GSK-beta (Abcam, ab107166) at 1:400, anti-MLC at 1:200, anti-phospho-MLC (Thermo) at 1:300, anti-ILK (ER 1592, Abcam 76468) at 1:800, anti-phospho-ILK (Millipore Ser 246, Ab1076) at 1:500, anti-vinculin (SPM22), anti-pFAK (BD pY397, cat#611722) at 1:600, and anti-p-c-src (sc9AC) at 1:100.

Imaging was conducted via PerkinElmer spinning disk confocal microscope using a 63X objective. Only isolated cells (those lacking contact with any other cells) were included in analysis. Where applicable, paxillin fluorescent signal was utilized to both identify the focal plane of imaging for cell adhesion as well as FA location and area. For determination of total F-actin content as well as total p-ILK and p-GSK content, confocal

z-stacks of 10-slices each spanning the entire cell thickness were acquired, and a summation of signal therein constituted a proxy of total protein content. Cell area or volume was determined from imaging of phalloidin staining (1:40) of either a 2D cell cross-sections (area) or 10 z-stack slices of cell cross-sections spanning the entire cell thickness (volume). Location of phalloidin stain was used to determine the cell edge, and Volocity software was used to fill in the space between theses edges and compute a total cell area or volume, as appropriate. Where indicated, normalized protein presence was determined by dividing total protein cellular content by total cellular area/volume, as appropriate. Nuclear volume was determined from hoesct signal. Image analysis, thresholding, and quantitation was performed using Volocity quantitation software.

Rac and Rho GLISAs

HFFs were plated at 10K cells/cm^2 in 100mm petri dishes pre-coated with FN or cFN and allowed to attach for 30 minutes before being collected, lysed, and analyzed using the Rac1 (BK128-S) or Rho (BK124-S) colorimetric GLISA assays from Cytoskeleton, Inc. Protein loading was normalized to total protein content determined according to 660nm protein quantification assay. A total of two plates of cells were prepared per substrate, with duplicate wells analyzed per sample. Each GLISA was performed twice.

Magnetic Bead Force-Inducible Co-Immunoprecipitation:

These assays were conducted as previously described by Fiore et. al.[66] and Guilluy et. al. [67]. Briefly, Invitrogen M-280 Tosylactivated Dynabeads were covalently bound to FN or cFN and subsequently blocked in hd-BSA using manufacturer recommended protocols. HFFs were plated at a density of 2.5 x 10^6 cells per 10cm petri dish and serum-starved 24 hours in Opti-MEM media. Protein-coated beads were allowed to incubate with cells for 1 hour. Attachment of FN/cFN-coated beads to plated cells and the integrin interactions therein represent the no-force condition. The +Force condition was achieved through application of a magnet from a distance of 20mm which effectively pulled on the magnetic beads bound to cells with a force of ~10pN each. Unbound beads were washed away with cold PBS solution, after which the remaining beads were collected via cell scraping and addition of lysis buffer. Protein loading for SDS PAGE and subsequent western blotting was normalized using Pierce 660nm Protein Assay Reagent. The following antibodies were utilized for western blot analysis: anti-αv H075 integrin from sant cruz (sc-10719), anti-a5 (AB1928), anti p-ILK ser246 (AB1076), and anti-paxillin Y113 (ab32084) from abcam, anti-p-src D49G4, anti-src 32G6, and anti-ILK (#3862) from cell signaling, anti-pFAK 44-624G from thermo fischer, and anti-FAK pY397 from BD Biosciences. Appropriate mouse or rabbit horse radish peroxidase (HRP)-conjugated antibodies were utilized for secondary staining. Chemiluminescent western blot signals within a linear range of exposure were read and interpreted using a GE Amersham Imager 600.

AFM Analysis of Cell Stiffness:

HFFs were plated on cFN/FN-coated glass coverslips for 1 hour in SFM at which point 2.73μm beaded AFM tips (Bruker MCLT-O10) were used to indent two unique locations per cell for a total of 50 cells per substrate over two dishes each with an Asylum MFP-3D AFM with inverted Nikon light microscope. A subset of cells were subsequently fixed with paraformadahyde and re-assayed as a positive stiffness control. Cell plating was staggered such that all cells were assayed within two hours of initial plating. For evaluation of Young's bulk modulus when plated on variable stiffness substrates, an identical procedure was followed using Matrigen EasyCoat gel-coated coverslips of defined stiffness of 1kPa or 9kPa. Gel stiffness was confirmed by directly indenting a 1mm region of the gels.

Traction force microscopy:

Traction force microscopy was performed as previously described [68]. Briefly, PDMS (Sylgard) was mixed in a 1:10 ratio of elastomer to base and degassed for 30 min before pouring onto the micropatterned Su-85 mold. After incubation at 80^{o}C for at least 4 hours, the PDMS stamp were then cut out of the mold, plasma-treated and coated with 125ul 100ug/mL alex488 conjugated human fibronectin or citrullinated human fibronectin for 1 hour. The patterns were then transferred onto plasma-treated coverglasses. A drop (35ul) of 13.6 Kpa polyacrylamide (PAA) gel containing 0.2% Acrylic acid N-hydroxysuccinimide ester (Sigma-Aldrich) was placed between the patterned coverglass and a base coverglass which was previously treated with 5% (3-

Aminopropyl) triethoxysilane and 0.5% glutaraldehyde to form a "sandwiched" structure. The coverglass with micropatterned human fibronectin was carefully peeled off after the gel completely polymerized and the pattern was now transferred on the PAA gel. The patterned PAA gel was then placed inside a sterilized Atto Fluor cell chamber (Thermo Fisher Scientific) and covered with 1mL 1% pen/strep in PBS (Gibco) for 8 hours under 4^{o}C. The cell chamber was then coated with serum-free Opti-MEM medium (Thermo Fisher Scientific) for 40 min under 37 ^{o}C. After medium exchange $5*10^5$ human foreskin fibroblasts (HFF) were seeded on to the patterned PAA gel and cultured under 37 ^{o}C for 2 hours. Afterward, the cell chamber was imaged by a 40x, 1.25 N.A. water immersion objective (Nikon) with a spinning disk confocal microscope system (Perkin Elmer). Each cell was imaged 25 times sequentially with 60s interval. From at least three independent assays, a total 30 cells were imaged from either normal human fibronectin or citrullinated human fibronectin patterned PAA gels. The sequential images were stacked in ImageJ and analyzed by a Matlab script kindly provided by Dr. Michael Smith (Boston University).

Alpha-actinin Assays:

HFFs were plated in SFM for 2 hours on coverslips pre-coated with FN or cFN. For negative controls of FA turnover, cells were plated on FN in the presence of 10uM PF-28 for the full 2 hours or 2uM of cytochalasin D for the last 30 minutes of cell plating. After 2 hours, cells were washed, fixed in paraformaldehyde, and stained with anti-α-actinin (ab18061, Abcam) at 1:400, anti- rabbit paxillin (ab32084, abcam), and phalloidin. Only individual cells determined not to be in contact with any neighboring cells were imaged via PerkinElmer spinning disk confocal microscope using a 63X objective. A total of 75 cells over 4 coverslips were imaged per condition. Three biological replicates were performed, only one of which included sh-RNA β1 knockdown cells on FN or cFN as additional groups.

Real-Time Paxillin Turnover Analysis:

Low passage HFFs were transfected with RFP-paxillin (a kind gift from the Cassanova Lab at UVA), using 6μg per 200K cells along with 24μL of X-tremeGene Transfection Reagent (Sigma-Aldrich). Cells were allowed 14 hours for transfection, after which they were washed multiple times and provided fresh media. Cells were allowed to rest 24-hours in full-serum media before being plated on FN/cFN coated coverslip-bottom petri dishes (FluoroDish) in serum-free media supplemented with 25mM HEPEEs. Cells were allowed to adhere for two hours, at which point they were washed, given fresh SFM+ 25mM HEPES, and imaged via TIRF confocal microscopy within a temperature-controlled environmental chamber. FA turnover videos consisted of images taken once every 10 seconds for a total duration of 10 minutes per cell. Cell plating was staggered such that all cells were imaged within four hours of initial plating. A total of 14 cells were imaged per substrate across four separate dishes representing two biological replicates of unique RFP-paxillin transfection. Only isolated cells (those not touching any others) were imaged. FA turnover was quantified using Volocity quantitation software.

Random Migration Assays;

Cell culture dishes were divided in half using thin PDMS inserts adhered to the bottom utilizing silicone glue and allowed to dry 24 hours. Dishes were sterilized via UV radiation prior to coating the two halves with 20μg/mL FN or cFN protein in PBS overnight at 4^{o}C, after which plates were blocked with 1% hd-BSA. HFFs were plated at 4000 cells/cm^2 and given two hours to adhere before exchanging media for fresh SFM supplemented with 1% BSA. The divided 35mm dishes were placed within the 37^{o}C, CO_2-supplemented cell culture chamber of a Nikon Biostation imaging apparatus, and cell migration was monitored for the next 20 hours with 10x phase contrast images captured once every 10 minutes of nine unique fields of view on each substrate. Cell movements were quantitated using the cell tracker plugin of Image J. Persistence distance is defined as the cumulative distance travelled by a single cell without a change of direction greater than or equal to 90 degrees. Only cells for which the entire nucleus was visible for a minimum of 20 frames were included in analysis for a total of at least 90 cells per condition.

In vitro Wound Healing Assays:

Wound healing assays were conducted utilizing the CytoSelect 24-well Wound Healing Assay (Cell BioLabs, Inc.). Individual wells (n=4 per substrate) were coated with 50μg/mL fibrinogen (Fib) or 20μg/mL FN/cFN overnight at 4°C, and subsequently blocked with hd-BSA for 1 hour. HFFs were seeded at 200k cells/cm^2 around 0.9mm plastic inserts for 4 hours in SFM supplemented with 0.2% FN-depleted serum, after which inserts were removed, wells gently washed 2X with PBS, and fresh media was added. Following the 13 hour migration period cells were fixed in 4% PFA, stained with cresyl violet solution, and imaged via brightfield microscopy. Thresholding, contrast enhancement, and subsequent calculations of percent wound coverage were performed in ImageJ and Matlab with a total of 12 fields of view per substrate.

Floating Gel Contraction Assays:

Gels were prepared in non-TC 24 well plates pre-blocked in 2% hd-BSA, subsequently washed with PBS, and air-dried. FN-infused clots of 250μL volume were prepared with 2.5mg/mL fibrinogen, 200μg/mL FN, 1U/mL thrombin in HEPES/5mM $CaCl_2$ solution. Clots were allowed to polymerize for 30 minutes at 37°C, after which 500μL 1X citrullination buffer (with/without 10U/mg protein PAD4 + 11.2μg/mg protein PAD) was added for a 24hr incubation culminated with quenching in 20mM EDTA. N=12 each FN/cFN gels. Gels were washed 2X in PBS buffer before seeding cells.

HFFs were plated at 40,000 cells per well in 1mL SFM supplemented with 0.2% FN-depleted serum and aprotinin. Cells in latrunculin wells were allowed to attach for 1 hour before the addition of 12uM latrunculin. All cells were allowed a total of 4 hours for gel attachment before gels were detached from well walls using 30 gauge needles. Wells were imaged at 24 hours post gel detachment from walls, both before and after fixation with paraformaldehyde to confirm that fixation did not impact results. Fixed gels were subsequently washed 3X in PBS, stained in Ponceau solution for 30 minutes for enhanced contrast and washed a final time with water.

Strained Gel Contraction Assays:

Gels were prepared as described in the floating gel contraction assay. HFFs were plated at 30,000 cells/well in 1mL SFM supplemented with 0.2% FN-depleted serum + aprotinin per well. Media was replaced after first 24 hours. At the 48-hour timepoint, clots were released from well bottoms using a 30G needle around the gel edge and allowed to contract for 15minutes at which point they were photographed. They were then fixed in 4% PFA for 15minutes, washed 3X in PBS, stained with Pierce 660nm Assay Reagent for 15 minutes (for contrast), washed again in PBS, and finally imaged via flash photography. Image J was utilized to make measurements of final clot areas in photos both before and after fixation/staining. Twelve clots each were analyzed with or without citrullination. For no-contraction controls, non-citrullinated gels (n=5 each) were either exposed to media without cells or dosed with 12uM latrucuin B added 3 hours following initial cell seeding and replaced after the initial 24 hours.

In vivo dermal wound healing:

Human Fibrinogen (FIB3, Enzyme Research Laboratories), Thrombin from bovine plasma (T4648-1KU, Sigma-Aldrich), Factor XIII peptide FKGGERCG (Genscript), Calcium Chloride (97062 590, VWR) where purchased and used after filtering through a 0.22 um filter.

Female SKH-1 Elite mice (8 weeks old) and male SKH-1 Elite mice (7 weeks old) were purchased from Charles River and housed in a centralized animal facility at Duke University. All procedures were approved by the Duke University Institutional Animal Care and Use Committee and were in compliance with the NIH Guide for the Care and Use of Laboratory Animals.

The crosslinker solution (Thrombin/FXIII/$CaCl_2$) was incubated for half an hour before use and kept in a 37-degree heat block throughout the surgery. The excisional splinted wound protocol was an established protocol previously reported by others and is detailed by our previous publications [69, 70]. Briefly, young adult (7–12-week old mice) (Charles River Laboratories) were acclimated to the environment for five to seven days upon delivery prior to the procedure. Mice were individually anesthetized with 4% isoflurane and maintained at 1.5–2% isoflurane during surgery. Buprenorphine SR (one dosage of 1 mg/mL, 0.5 μg per g of mouse weight administered before surgery, which has a sustained effect for 72 hours) was injected

subcutaneously. The dorsal surface was sterilized with iodine and ethanol before surgery on an aseptic pad atop warming heat pads. Using sterile biopsy punches 5 mm wide, four clean, well-defined wounds were created slightly on the middle of the animal's back. Aseptic silicon ring splints with an 8-mm wide window were first glued to the wound with cyanoacrylate-based adhesive. 6 interrupted sutures were then made around each splint to prevent healing from loose skin contraction and allow for healing through re-epithelialization and granulation, which mimics the response in humans and fixed-skinned mammals[69]. The hydrogel components were mixed and immediately applied to the wounds. After 30-minute gelation time, circular shape Tegaderm dressings were adhered on top of each splint to prevent the wounds from drying out. Another layer of Teflon pad was place on top of the wounds and animals were carefully wrapped with another layer of a self-adhering elastic bandage (VetWrap, 3M, Inc.) to stop them from crewing off the splints. These animals were then monitored until awakening and housed individually in cages.

Right after wounding and on day 3, day 5, day 7 post-surgery, animals were re-wrapped, and pictures of the wounds were taken. On day 7, animals were euthanized, and wounded tissues were cut out and halved, where one half was fixed with 4% paraformaldehyde (PFA) overnight at 4 °C before paraffin embedding. Paraffin sections were sliced into 5 μm thickness for hematoxylin and eosin (H&E) stain and Trichrome stain. Animals were assigned randomly, and all tissue analysis was performed in a blind manner.

Wound closure was determined by: 1) quantification from the wound images, comparing the pixel area of the wound to the pixel area within the 8-mm centre hole of the rubber splint to get the wound size at different time points. Closure fractions were normalized to Day 0 for each wound. 2) quantification from the H&E staining, comparing the pixel length of the distance between the epithelial gap to the pixel length of the distance between the underlying muscle layer to get the closure fractions at day 7.

For all the stained slides, full wound scans were performed using ZEISS Axio Scan.Z1. Images were quantified in Image J for granulation tissue thickness and collagen percentage in granulation tissue. The quantification of cell density was performed with the Halo Next Generation Imaging analysis software (Indica Labs; Corrales, NM). HALO measures and reports individual cell data maintaining an interactive link between cell metrics and cell images. The number of infiltrating cells within the wound bed was automatically counted from H&E staining with the Halo software.

RA sera screening:

All RA cases fulfilled the 1987 American College of Rheumatology (ACR) classification criteria[71]. A screening cohort was examined from a previously published study with informed consent and ethical approval; the cohort comprised 22 British RA patients and 23 healthy individuals [72]. Peptides from fibronectin (P02751) were synthesized with C- and N-terminal cysteines (Pepceuticals) and solubilized in distilled water (FN1410, cFN1410, FN1452), 10% DMSO (cFN1434, cFN1452, FN1476/9, cFN1476/9) or 20% DMSO (FN1434) in distilled water at 10 mg/ml (Supplementary Table 1). ELISAs were used to detect antibodies against citrullinated peptides in human sera as described [73]. Briefly, 96-well Nunc Maxisorp plates were coated with 10 μg/mL peptide in coating buffer, blocked with 2% BSA and incubated with sera diluted 1:100. Bound antibodies were detected with an HRP-conjugated anti-human IgGFc monoclonal antibody (6043HRP, Stratech).

Statistical Analysis:

All statistical analysis was performed using GraphPad Prism software with 2-tailed t-tests or one-way ANOVAs and Tukey post-hoc analysis, as appropriate for the experimental set-up. Alpha was set at 0.05 for all analyses. In the case of larger data-sets, such as with fluorescent signal analysis of cell components in microscopy images, outliers were removed using the ROUT method with a Q of 1% prior to further statistical analyses. The Shapiro-Wilk test was utilized to test for normality of data distribution, and in cases where null hypothesis was rejected, the Mann-Whitney test was applied to ascertain statistical significance. Measurement of wound closure, granulation tissue thickness and collagen percentage in the samples were conducted with Fiji version 2. Peptide ELISA Positivity in the RA sera screen was defined by the cut-off of the 98% percentile of healthy control samples and Spearman correlations in addition to tests for statistical significance were performed.

The datasets generated and/or analyzed during the current study are available from the corresponding author on reasonable request.

Author Contributions:
VLS was primarily responsible for citrullination verification, CHO cell adhesion, ICC, Rac and Rho, FA turnover, cell migration, and gel contraction experiments. SC and MT performed MS and subsequent analyses. DMC carried out AFM experiments. PH conducted the traction force microscopy measurements. WL performed focal adhesion integrin ratio analysis. VY was primarily responsible for magnetic Co-IP experiments. KP assisted in cell migration experiments. YL performed the dermal wound healing experiments. AS conducted the RA sera screen. THB, MT, TS, KM contributed to experimental design, analysis, and manuscript preparation.

Acknowledgements:
This research was supported by the NSF GRFP and the NIH 5 F31 HL131274 to VLS, NIH R01 GM117400 to MT, NIH R01 NS079691 to TS, as well as NIH R01 HL127283 to THB. AS and KM were supported by a Senior Research Fellowship (20003) from Versus Arthritis. At Georgia Tech we thank the Sulchek lab and the Optical Microscopy Core facility (Dr. Aaron Lifland) for their respective technical assistance with AFM and confocal microscopy. At the University of Virginia our gratitude goes to the Cassanova lab for their donation of RFP-paxillin plasmids. At Duke University, we thank Dr. Lucas Schirmer and Lindsay Riley for their technical assistance. We would like to additionally thank Dr. Michael Smith and Han Xu (Boston University) for their assistance with traction force microscopy.

REFERENCES

[1] T. H. Barker and A. J. Engler, "The provisional matrix: setting the stage for tissue repair outcomes," *Matrix Biol,* vol. 60-61, pp. 1-4, Jul 2017.
[2] B.-H. Gu, M. C. Madison, D. Corry, and F. Kheradmand, "Matrix remodeling in chronic lung diseases," *Matrix Biology,* vol. 73, pp. 52-63, 2018/11/01/ 2018.
[3] R. V. Iozzo and M. A. Gubbiotti, "Extracellular matrix: The driving force of mammalian diseases," *Matrix biology : journal of the International Society for Matrix Biology,* vol. 71-72, pp. 1-9, 2018/10// 2018.
[4] A. Neve, F. P. Cantatore, N. Maruotti, A. Corrado, and D. Ribatti, "Extracellular Matrix Modulates Angiogenesis in Physiological and Pathological Conditions," *BioMed Research International,* vol. 2014, p. 756078, 05/18, 01/16/received, 02/27/accepted 2014.
[5] M. Ahmed and C. ffrench-Constant, "Extracellular Matrix Regulation of Stem Cell Behavior," *Current Stem Cell Reports,* vol. 2, pp. 197-206, 07/07 2016.
[6] Y. Zhou, J. C. Horowitz, A. Naba, N. Ambalavanan, K. Atabai, J. Balestrini, *et al.*, "Extracellular matrix in lung development, homeostasis and disease," *Matrix Biol,* vol. 73, pp. 77-104, Nov 2018.
[7] L. Sorokin, "The impact of the extracellular matrix on inflammation," *Nature Reviews Immunology,* vol. 10, p. 712, 09/24/online 2010.
[8] J. Fuhrmann and P. R. Thompson, "Protein Arginine Methylation and Citrullination in Epigenetic Regulation," *ACS Chemical Biology,* vol. 11, pp. 654-668, 2016/03/18 2016.
[9] J. E. Jones, C. P. Causey, B. Knuckley, J. L. Slack-Noyes, and P. R. Thompson, "Protein arginine deiminase 4 (PAD4): Current understanding and future therapeutic potential," *Current opinion in drug discovery & development,* vol. 12, pp. 616-27, Sep 2009.
[10] E. A. V. Moelants, A. Mortier, J. Van Damme, P. Proost, and T. Loos, "Peptidylarginine deiminases: physiological function, interaction with chemokines and role in pathology," *Drug Discovery Today: Technologies,* vol. 9, pp. e261-e280, //Winter 2012.
[11] C. Zeltz and D. Gullberg, "Post-translational modifications of integrin ligands as pathogenic mechanisms in disease," *Matrix Biol,* vol. 40C, pp. 5-9, Nov 2014.
[12] M. Gogol, "Citrullination--small change with a great consequence," in *Folia Biologica et Oecologica* vol. 9, ed, 2013, p. 17.

[13] Y. Zhou, B. Chen, N. Mittereder, R. Chaerkady, M. Strain, L.-L. An, *et al.*, "Spontaneous Secretion of the Citrullination Enzyme PAD2 and Cell Surface Exposure of PAD4 by Neutrophils," *Frontiers in Immunology,* vol. 8, p. 1200, 09/25, 07/28/received, 09/11/accepted 2017.

[14] X. Chang and J. Han, "Expression of peptidylarginine deiminase type 4 (PAD4) in various tumors," *Molecular carcinogenesis,* vol. 45, pp. 183-96, Mar 2006.

[15] S. Mohanan, B. D. Cherrington, S. Horibata, J. L. McElwee, P. R. Thompson, and S. A. Coonrod, "Potential role of peptidylarginine deiminase enzymes and protein citrullination in cancer pathogenesis," *Biochem Res Int,* vol. 2012, p. 895343, 2012.

[16] K. Antoniou, K. Samara, I. Lasithiotaki, P. Pantelidis, N. Siafakas, and A. Wells, "Investigation of the citrullination pathway in the pathogenesis of fibrotic lung disorders," *European Respiratory Journal,* vol. 40, September 1, 2012 2012.

[17] E. B. Lugli, R. E. Correia, R. Fischer, K. Lundberg, K. R. Bracke, A. B. Montgomery, *et al.*, "Expression of citrulline and homocitrulline residues in the lungs of non-smokers and smokers: implications for autoimmunity in rheumatoid arthritis," *Arthritis Res Ther,* vol. 17, p. 9, 2015.

[18] J. Koziel, P. Mydel, and J. Potempa, "The link between periodontal disease and rheumatoid arthritis: an updated review," *Curr Rheumatol Rep,* vol. 16, p. 408, Mar 2014.

[19] W. J. van Venrooij and G. J. Pruijn, "How citrullination invaded rheumatoid arthritis research," *Arthritis Res Ther,* vol. 16, p. 103, 2014.

[20] K. Shin, S. Hong, E.-H. Choi, M.-K. Lim, S.-C. Shim, J.-H. Ju, *et al.*, "Role of Citrullinated Fibrinogen Peptides in the Activation of CD4 T Cells from Patients with Rheumatoid Arthritis," *Immune Network,* vol. 13, pp. 116-122, 08/26, 06/13/received, 06/24/revised, 06/26/accepted 2013.

[21] J. Sokolove, X. Zhao, P. E. Chandra, and W. H. Robinson, "Immune complexes containing citrullinated fibrinogen costimulate macrophages via Toll-like receptor 4 and Fcgamma receptor," *Arthritis Rheum,* vol. 63, pp. 53-62, Jan 2011.

[22] J. A. Hill, D. A. Bell, W. Brintnell, D. Yue, B. Wehrli, A. M. Jevnikar, *et al.*, "Arthritis induced by posttranslationally modified (citrullinated) fibrinogen in DR4-IE transgenic mice," *J Exp Med,* vol. 205, pp. 967-79, Apr 14 2008.

[23] Y. T. Ting, J. Petersen, S. H. Ramarathinam, S. W. Scally, K. l. loh, R. Thomas, *et al.*, "The interplay between citrullination and HLA-DRB1 polymorphism in shaping peptide binding hierarchies in Rheumatoid Arthritis," *Journal of Biological Chemistry,* January 9, 2018 2018.

[24] M. Sebbag, N. Moinard, I. Auger, C. Clavel, J. Arnaud, L. Nogueira, *et al.*, "Epitopes of human fibrin recognized by the rheumatoid arthritis-specific autoantibodies to citrullinated proteins," *Eur J Immunol,* vol. 36, pp. 2250-63, Aug 2006.

[25] K. D. Samara, A. Trachalaki, E. Tsitoura, A. V. Koutsopoulos, E. D. Lagoudaki, I. Lasithiotaki, *et al.*, "Upregulation of citrullination pathway: From Autoimmune to Idiopathic Lung Fibrosis," *Respiratory research,* vol. 18, p. 218, 2017/12/29 2017.

[26] K. H. Sipilä, V. Ranga, P. Rappu, M. Mali, L. Pirilä, I. Heino, *et al.*, "Joint inflammation related citrullination of functional arginines in extracellular proteins," *Scientific Reports,* vol. 7, p. 8246, 2017/08/15 2017.

[27] J. J. van Beers, A. Willemze, J. Stammen-Vogelzangs, J. W. Drijfhout, R. E. Toes, and G. J. Pruijn, "Anti-citrullinated fibronectin antibodies in rheumatoid arthritis are associated with human leukocyte antigen-DRB1 shared epitope alleles," *Arthritis Res Ther,* vol. 14, p. R35, Feb 17 2012.

[28] S. D. Redick, D. L. Settles, G. Briscoe, and H. P. Erickson, "Defining Fibronectin's Cell Adhesion Synergy Site by Site-Directed Mutagenesis," *The Journal of Cell Biology,* vol. 149, pp. 521-527, 11/22/received, 02/23/rev-request, 03/09/accepted 2000.

[29] L. Cao, J. Nicosia, J. Larouche, Y. Zhang, H. Bachman, A. C. Brown, *et al.*, "Detection of an Integrin-Binding Mechanoswitch within Fibronectin during Tissue Formation and Fibrosis," *ACS nano,* vol. 11, pp. 7110-7117, Jul 25 2017.

[30] J. Schnittert, R. Bansal, G. Storm, and J. Prakash, "Integrins in wound healing, fibrosis and tumor stroma: High potential targets for therapeutics and drug delivery," *Advanced Drug Delivery Reviews,* 2018/02/04/ 2018.

[31] P. Costa, T. M. E. Scales, J. Ivaska, and M. Parsons, "Integrin-Specific Control of Focal Adhesion Kinase and RhoA Regulates Membrane Protrusion and Invasion," *PLOS ONE,* vol. 8, p. e74659, 2013.

[32] J. Franco-Barraza, R. Francescone, T. Luong, N. Shah, R. Madhani, G. Cukierman, *et al.*, "Matrix-regulated integrin α(v)β(5) maintains α(5)β(1)-dependent desmoplastic traits prognostic of neoplastic recurrence," *eLife,* vol. 6, p. e20600, 01/31, 08/14/received, 01/05/accepted 2017.

[33] M. Bharadwaj, N. Strohmeyer, G. P. Colo, J. Helenius, N. Beerenwinkel, H. B. Schiller, *et al.*, "αV-class integrins exert dual roles on α5β1 integrins to strengthen adhesion to fibronectin," *Nature Communications,* vol. 8, p. 14348, 01/27/online 2017.

[34] J. Solon, I. Levental, K. Sengupta, P. C. Georges, and P. A. Janmey, "Fibroblast Adaptation and Stiffness Matching to Soft Elastic Substrates," *Biophysical Journal,* vol. 93, pp. 4453-4461, 11/20/received, 06/21/accepted 2007.

[35] T. Yeung, P. C. Georges, L. A. Flanagan, B. Marg, M. Ortiz, M. Funaki, *et al.*, "Effects of substrate stiffness on cell morphology, cytoskeletal structure, and adhesion," *Cell Motility and the Cytoskeleton,* vol. 60, pp. 24-34, 2005.

[36] T. Sun, M. Rodriguez, and L. Kim, "Glycogen synthase kinase 3 in the world of cell migration," *Development, growth & differentiation,* vol. 51, pp. 735-42, Dec 2009.

[37] D. J. Webb, K. Donais, L. A. Whitmore, S. M. Thomas, C. E. Turner, J. T. Parsons, *et al.*, "FAK-Src signalling through paxillin, ERK and MLCK regulates adhesion disassembly," *Nat Cell Biol,* vol. 6, pp. 154-61, Feb 2004.

[38] A. K. Harris, D. Stopak, and P. Wild, "Fibroblast traction as a mechanism for collagen morphogenesis," *Nature,* vol. 290, p. 249, 03/19/online 1981.

[39] P. Roy, W. M. Petroll, C. J. Chuong, H. D. Cavanagh, and J. V. Jester, "Effect of Cell Migration on the Maintenance of Tension on a Collagen Matrix," *Annals of Biomedical Engineering,* vol. 27, pp. 721-730, 1999/11/01 1999.

[40] E. Girbal-Neuhauser, J.-J. Durieux, M. Arnaud, P. Dalbon, M. Sebbag, C. Vincent, *et al.*, "The Epitopes Targeted by the Rheumatoid Arthritis-Associated Antifilaggrin Autoantibodies are Posttranslationally Generated on Various Sites of (Pro)Filaggrin by Deimination of Arginine Residues," *The Journal of Immunology,* vol. 162, p. 585, 1999.

[41] G. A. Schellekens, B. A. de Jong, F. H. van den Hoogen, L. B. van de Putte, and W. J. van Venrooij, "Citrulline is an essential constituent of antigenic determinants recognized by rheumatoid arthritis-specific autoantibodies," *The Journal of clinical investigation,* vol. 101, pp. 273-281, 1998.

[42] H. E. Balcioglu, H. van Hoorn, D. M. Donato, T. Schmidt, and E. H. Danen, "The integrin expression profile modulates orientation and dynamics of force transmission at cell-matrix adhesions," *J Cell Sci,* vol. 128, pp. 1316-26, Apr 1 2015.

[43] E. Cukierman, R. Pankov, D. R. Stevens, and K. M. Yamada, "Taking cell-matrix adhesions to the third dimension," *Science,* vol. 294, pp. 1708-12, Nov 23 2001.

[44] P. Roca-Cusachs, N. C. Gauthier, A. Del Rio, and M. P. Sheetz, "Clustering of alpha(5)beta(1) integrins determines adhesion strength whereas alpha(v)beta(3) and talin enable mechanotransduction," *Proc Natl Acad Sci U S A,* vol. 106, pp. 16245-50, Sep 22 2009.

[45] H. B. Schiller, M. R. Hermann, J. Polleux, T. Vignaud, S. Zanivan, C. C. Friedel, *et al.*, "beta1- and alphav-class integrins cooperate to regulate myosin II during rigidity sensing of fibronectin-based microenvironments," *Nat Cell Biol,* vol. 15, pp. 625-36, Jun 2013.

[46] J. C. Friedland, M. H. Lee, and D. Boettiger, "Mechanically activated integrin switch controls alpha5beta1 function," *Science,* vol. 323, pp. 642-4, Jan 30 2009.

[47] M. A. Shelef, D. A. Bennin, D. F. Mosher, and A. Huttenlocher, "Citrullination of fibronectin modulates synovial fibroblast behavior," *Arthritis Res Ther,* vol. 14, p. R240, 2012.

[48] J. Takagi, K. Strokovich, T. A. Springer, and T. Walz, "Structure of integrin alpha5beta1 in complex with fibronectin," *The EMBO journal,* vol. 22, pp. 4607-4615, 2003.

[49] E. Darrah and F. Andrade, "Rheumatoid arthritis and citrullination," *Current opinion in rheumatology,* vol. 30, pp. 72-78, 2018.

[50] D. J. Webb, K. Donais, L. A. Whitmore, S. M. Thomas, C. E. Turner, J. T. Parsons, *et al.*, "FAK–Src signalling through paxillin, ERK and MLCK regulates adhesion disassembly," *Nature Cell Biology,* vol. 6, p. 154, 01/25/online 2004.

[51] X.-K. Zhao, Y. Cheng, M. Liang Cheng, L. Yu, M. Mu, H. Li, *et al.*, "Focal Adhesion Kinase Regulates Fibroblast Migration via Integrin beta-1 and Plays a Central Role in Fibrosis," *Scientific Reports,* vol. 6, p. 19276, 01/14/online 2016.

[52] C. Bergmann, A. Akhmetshina, C. Dees, K. Palumbo, P. Zerr, C. Beyer, *et al.*, "Inhibition of glycogen synthase kinase 3beta induces dermal fibrosis by activation of the canonical Wnt pathway," *Ann Rheum Dis,* vol. 70, pp. 2191-8, Dec 2011.

[53] L. Fan, Q. Wang, R. Liu, M. Zong, D. He, H. Zhang, *et al.*, "Citrullinated fibronectin inhibits apoptosis and promotes the secretion of pro-inflammatory cytokines in fibroblast-like synoviocytes in rheumatoid arthritis," *Arthritis Res Ther,* vol. 14, p. R266, 2012.

[54] K. Sipila, S. Haag, K. Denessiouk, J. Kapyla, E. C. Peters, A. Denesyuk, *et al.*, "Citrullination of collagen II affects integrin-mediated cell adhesion in a receptor-specific manner," *FASEB J*, vol. 28, pp. 3758-68, Aug 2014.

[55] P. R. Sonavane, C. Wang, B. Dzamba, G. F. Weber, A. Periasamy, and D. W. DeSimone, "Mechanical and signaling roles for keratin intermediate filaments in the assembly and morphogenesis of Xenopus mesendoderm tissue at gastrulation," *Development (Cambridge, England)*, vol. 144, pp. 4363-4376, Dec 1 2017.

[56] Q. Shi and D. Boettiger, "A Novel Mode for Integrin-mediated Signaling: Tethering Is Required for Phosphorylation of FAK Y397," *Molecular Biology of the Cell*, vol. 14, pp. 4306-4315, 01/27/received, 05/07/revised, 07/01/accepted 2003.

[57] J. Roman, J. D. Ritzenthaler, S. Roser-Page, X. Sun, and S. Han, "α5β1-Integrin Expression Is Essential for Tumor Progression in Experimental Lung Cancer," *American Journal of Respiratory Cell and Molecular Biology*, vol. 43, pp. 684-691, 10/12/received, 01/11/accepted 2010.

[58] J. S. Knight, W. Luo, A. A. O'Dell, S. Yalavarthi, W. Zhao, V. Subramanian, *et al.*, "Peptidylarginine deiminase inhibition reduces vascular damage and modulates innate immune responses in murine models of atherosclerosis," *Circ Res*, vol. 114, pp. 947-56, Mar 14 2014.

[59] J. Kawalkowska, A.-M. Quirke, F. Ghari, S. Davis, V. Subramanian, P. R. Thompson, *et al.*, "Abrogation of collagen-induced arthritis by a peptidyl arginine deiminase inhibitor is associated with modulation of T cell-mediated immune responses," *Scientific Reports*, vol. 6, p. 26430, 05/23/online 2016.

[60] J. S. Knight, V. Subramanian, A. A. O'Dell, S. Yalavarthi, W. Zhao, C. K. Smith, *et al.*, "Peptidylarginine deiminase inhibition disrupts NET formation and protects against kidney, skin and vascular disease in lupus-prone MRL/lpr mice," *Ann Rheum Dis*, vol. 74, pp. 2199-206, Dec 2015.

[61] A. Sarswat, E. Wasilewski, S. K. Chakka, A. M. Bello, A. V. Caprariello, C. M. Muthuramu, *et al.*, "Inhibitors of protein arginine deiminases and their efficacy in animal models of multiple sclerosis," *Bioorganic & medicinal chemistry*, vol. 25, pp. 2643-2656, May 1 2017.

[62] A. A. Chumanevich, C. P. Causey, B. A. Knuckley, J. E. Jones, D. Poudyal, A. P. Chumanevich, *et al.*, "Suppression of colitis in mice by Cl-amidine: a novel peptidylarginine deiminase inhibitor," *Am J Physiol Gastrointest Liver Physiol*, vol. 300, pp. G929-38, Jun 2011.

[63] E. E. Witalison, X. Cui, C. P. Causey, P. R. Thompson, and L. J. Hofseth, "Molecular targeting of protein arginine deiminases to suppress colitis and prevent colon cancer," *Oncotarget*, vol. 6, pp. 36053-62, Nov 3 2015.

[64] M. Knipp and M. Vasak, "A colorimetric 96-well microtiter plate assay for the determination of enzymatically formed citrulline," *Anal Biochem*, vol. 286, pp. 257-64, Nov 15 2000.

[65] A. Shevchenko, H. Tomas, J. Havlis, J. V. Olsen, and M. Mann, "In-gel digestion for mass spectrometric characterization of proteins and proteomes," *Nat Protoc*, vol. 1, pp. 2856-60, 2006.

[66] V. F. Fiore, P. W. Strane, A. V. Bryksin, E. S. White, J. S. Hagood, and T. H. Barker, "Conformational coupling of integrin and Thy-1 regulates Fyn priming and fibroblast mechanotransduction," *J Cell Biol*, vol. 211, pp. 173-90, Oct 12 2015.

[67] C. Guilluy, V. Swaminathan, R. Garcia-Mata, E. Timothy O'Brien, R. Superfine, and K. Burridge, "The Rho GEFs LARG and GEF-H1 regulate the mechanical response to force on integrins," *Nature Cell Biology*, vol. 13, p. 722, 05/15/online 2011.

[68] S. R. Polio, K. E. Rothenberg, D. Stamenovic, and M. L. Smith, "A micropatterning and image processing approach to simplify measurement of cellular traction forces," *Acta Biomater*, vol. 8, pp. 82-8, Jan 2012.

[69] R. D. Galiano, V. Michaels, Joseph, M. Dobryansky, J. P. Levine, and G. C. Gurtner, "Quantitative and reproducible murine model of excisional wound healing," *Wound Repair and Regeneration*, vol. 12, pp. 485-492, 2004.

[70] S. Zhu, S. Li, H. Escuin-Ordinas, R. Dimatteo, W. Xi, A. Ribas, *et al.*, "Accelerated wound healing by injectable star poly(ethylene glycol)-b-poly(propylene sulfide) scaffolds loaded with poorly water-soluble drugs," *Journal of Controlled Release*, vol. 282, pp. 156-165, 2018/07/28/ 2018.

[71] F. C. Arnett, S. M. Edworthy, D. A. Bloch, D. J. McShane, J. F. Fries, N. S. Cooper, *et al.*, "The American Rheumatism Association 1987 revised criteria for the classification of rheumatoid arthritis," *Arthritis Rheum*, vol. 31, pp. 315-24, Mar 1988.

[72] K. Lundberg, A. Kinloch, B. A. Fisher, N. Wegner, R. Wait, P. Charles, *et al.*, "Antibodies to citrullinated α-enolase peptide 1 are specific for rheumatoid arthritis and cross-react with bacterial enolase," *Arthritis & Rheumatism*, vol. 58, pp. 3009-3019, 2008.

[73] A. Schwenzer, X. Jiang, T. R. Mikuls, J. B. Payne, H. R. Sayles, A.-M. Quirke, *et al.*, "Identification of an immunodominant peptide from citrullinated tenascin-C as a major target for autoantibodies in rheumatoid arthritis," *Annals of the Rheumatic Diseases*, vol. 75, pp. 1876-1883, 2016.

Figure 1

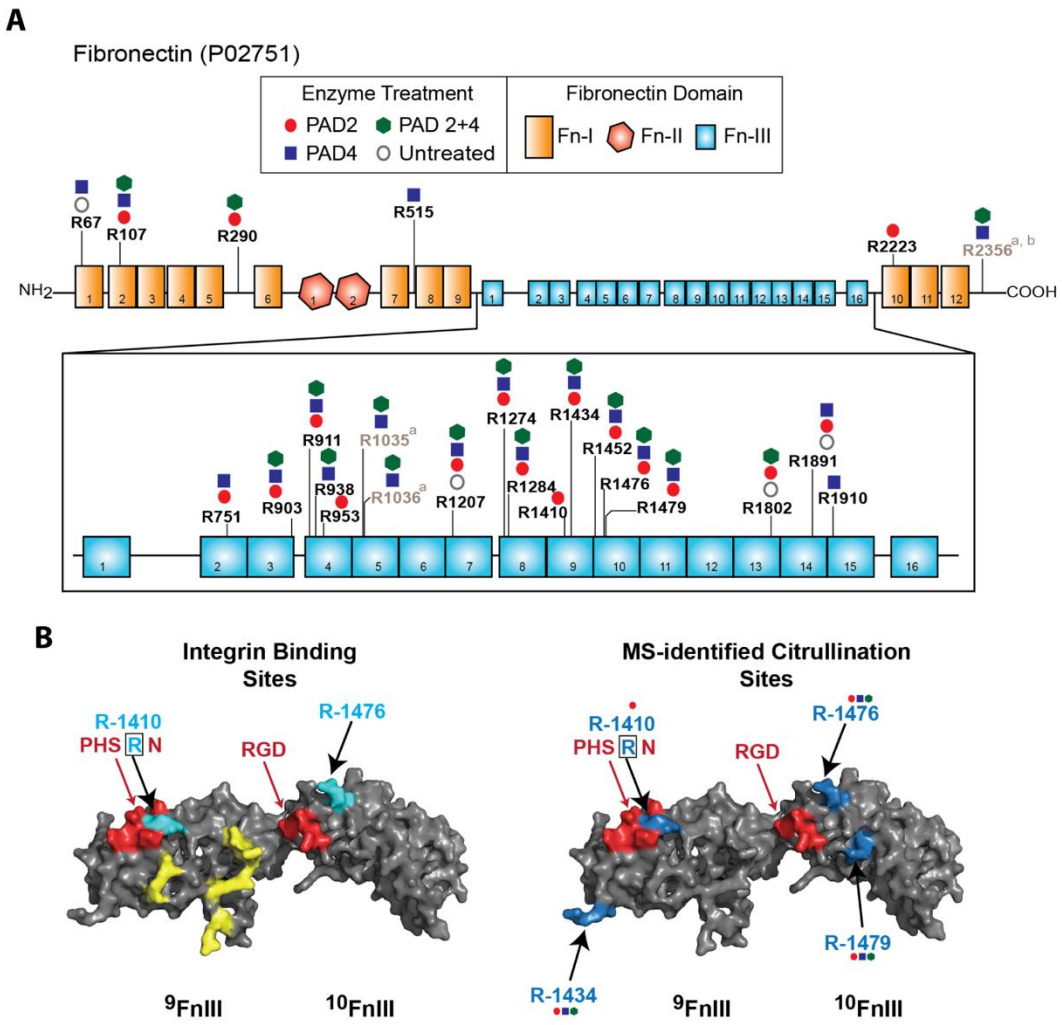

Figure 1: Mapping citrullination sites on human fibronectin. (A) Schematic overview of citrullination sites mapped onto human FN comprised of repetitive units of type I-III domains (depicted in different shapes). Tandem mass spectrometry was used to map the positions of citrullinated residues in purified plasma FN, which were either untreated or subjected to *in vitro* enzymatic citrullination by PAD2, PAD4, or both. Three previously reported sites (R1035, R1036, and R2356) that were also detected here are shown (residue labeled in brown) ((a) van Beer et. al. 2012[27]; (b) K. Sipila et. al. 2017[26]). (B) Three-dimensional structure of the 9th and 10th fibronectin type III domain (PDB 4LXO) highlighting residues previously shown to be essential for integrin binding (Redick et al, 2000[28]) (Left). (Red) RGD and PHSRN sequences essential for synergistic integrin binding. (Cyan) residues with the greatest degree of binding influence outside the RGD site (R1410 and R1476). (Yellow) residues that help to facilitate PHSRN interactions. (Right) MS-identified citrullination sites within the $^{9\text{-}10}$FNIII domains showing overlap with integrin binding residues R1410 and R1476, as well as additional sites near the integrin binding interface (R1434, R1479) and R1452 (underneath R1476 and not shown here).

Figure 2

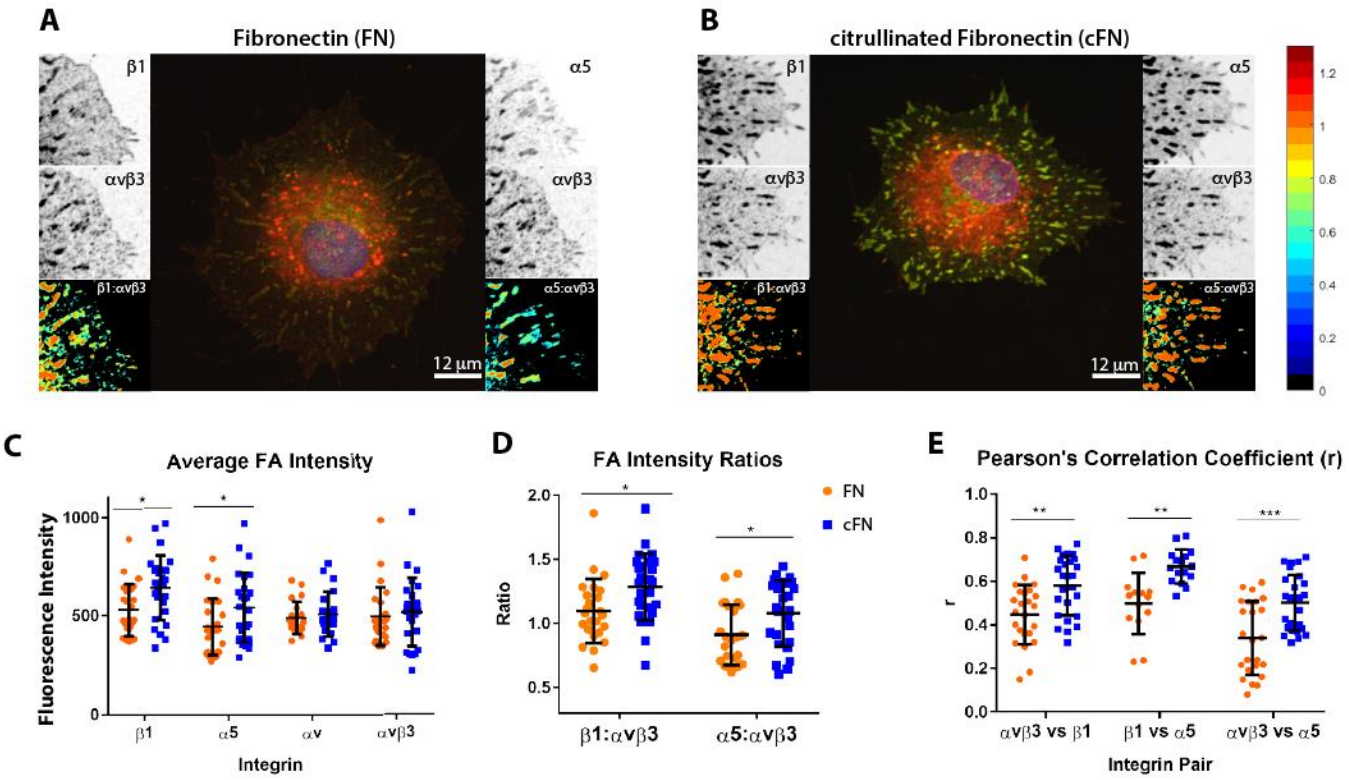

Figure 2: Fibroblasts exposed to cFN demonstrate an αvβ3 to α5β1 integrin switch and clustering. Fluorescence quantification from confocal images of HFFs (n = 20 cells per substrate) stained for individual integrin subunits provide a measure of average integrin fluorescent intensity within FAs (C, *p=0.01, *p=0.04, 0.5, and 0.6 left to right) and ratios of integrin intensity (D) both indicating a preference for α5β1 integrins on cFN (*p=.01 and .02 left to right). (E) Pearson's correlation coefficient for each pairwise comparison of integrin signal. (E, *p=.002, **p=.001) indicates enhanced integrin clustering on cFN. Error bars in C-E represent SD.

Figure 3

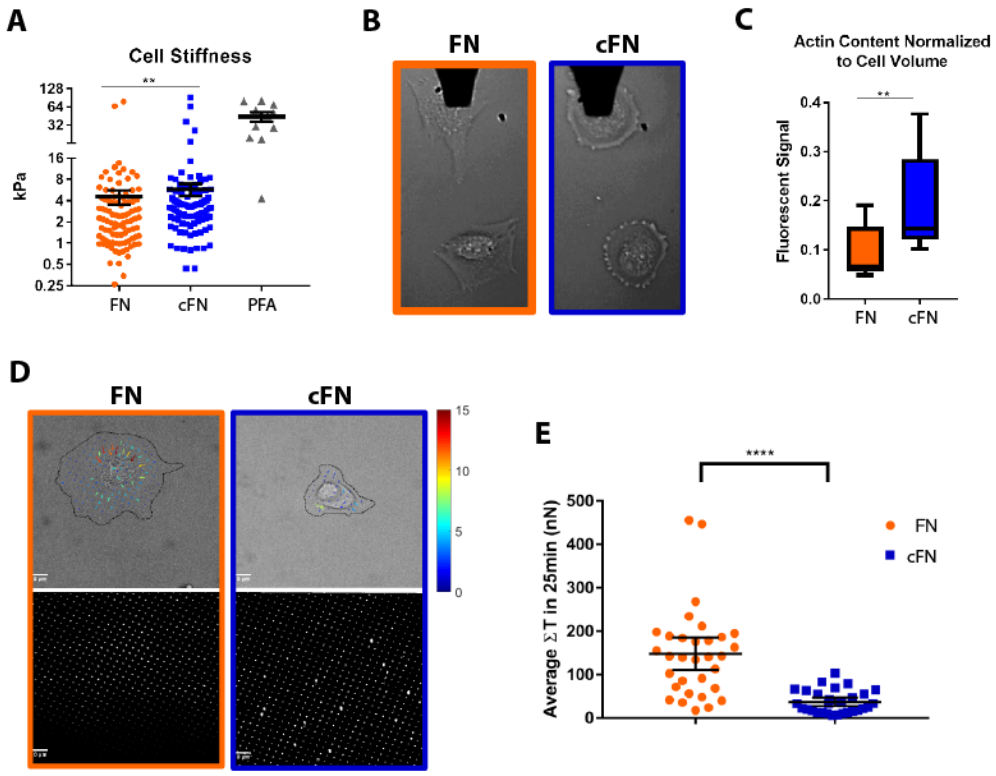

Figure 3: Fibroblasts exposed to cFN artificially enter a mechanically stressed state. Due to "stiffness-matching" abilities of fibroblasts, AFM was employed to decode their stiffness perception of cFN or FN-coated glass coverslips. Analysis of two distinct locations from 50 cells each per substrate is quantified in (A, mean ± SEM, **p = 0.0076 Mann-Whitney) showing higher average stiffness values on cFN, despite the generally smaller and more rounded appearance of the cells, as seen in representative AFM phase images in (B). Positive stiffness controls were paraformaldehyde (PFA)-treated cells. (C) Quantification of total F-actin content normalized to cell volume (n = 20 cells/substrate) as measured from confocal z-stacks of phalloidin- stained cells shows enhancements on cFN, a further indication of active mechanosensing.

Figure 4

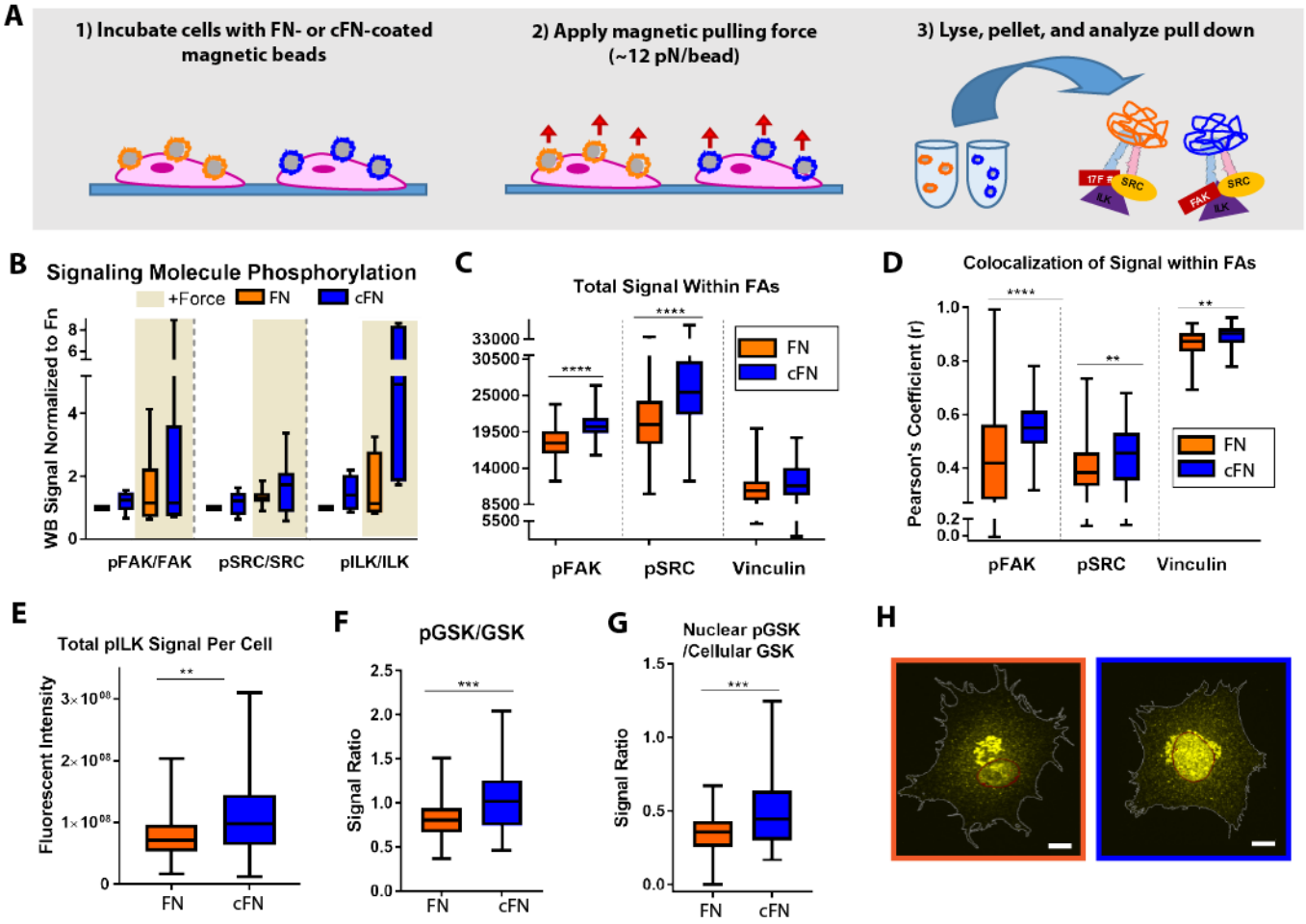

Figure 4: β1-Dominant Integrin Expression on cFN promotes force-sensitive downstream signaling.
The basic protocol for the force-inducible magnetic bead Co-IP experiments is shown in (A) with WB measurements for pFAK/FAK (n=7), pSRC/SRC (n=7), and pILK/ILK (n=4), all normalized to the condition of FN-coated beads without force are shown in (B). Light brown background shading indicates beads exposed to magnetic force (+force) whereas white backgrounds indicate no magnetic force was applied. Fluorescent signal from IF staining was quantified to reveal the total signal (C) and co-localization (D) within FAs of pFAK, pSrc, and vinculin (70 cells/substrate). Quantification of total pILK content per cell (E)(n = 50 cells per substrate), total pGSK/GSK (F), and total nuclear pGSK/cellular GSK (G) (n = 70 cells per substrate) as measured from confocal z-stacks of pILK- or pGSK/GSK-stained cells, as appropriate, shows enhancements of each metic on cFN compared to FN. All error bars represent min/max. Representative maximum intensity projections of pGSK-stained cells are shown in (H) with the p-GSK signal in yellow, nucleus outlined in red, and the cell edge in white. Results are non-significant unless otherwise indicated.

Figure 5

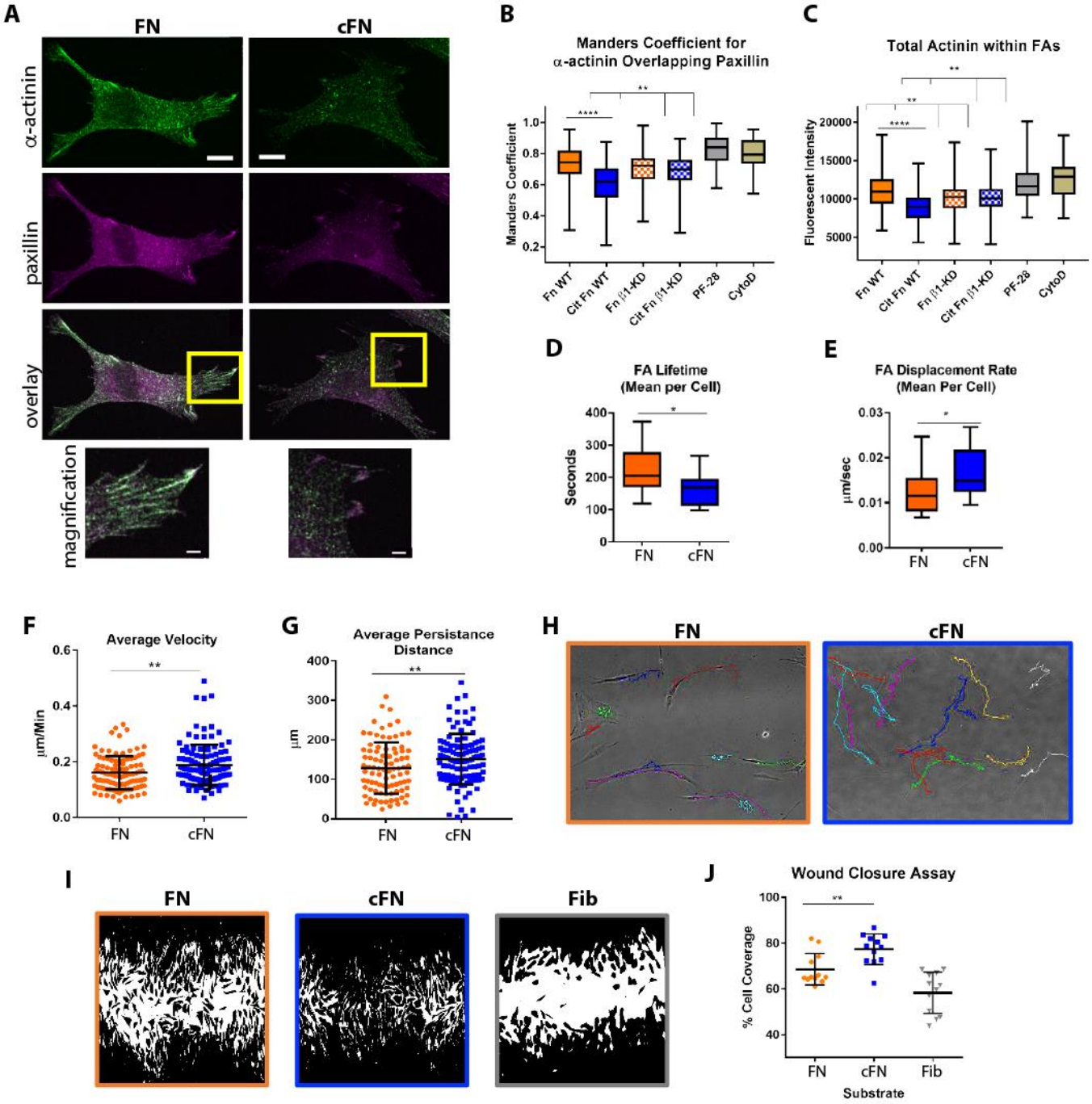

Figure 5: Fibroblasts display increased FA turnover and migration on cFN. HFFs were stained with α-actinin as a proxy marker for stable FAs. Representative spinning disk confocal images (A) of HFFs on FN (left) or cFN (right) with staining for α-actinin in green, paxillin in magenta, and overlay highlight less co-localization of fluorescent signal within cells plated on cFN (Pearson's r = 0.523) indicating less stable adhesions compared to cells on FN (pearson's r = 0.822). Scale bar = 13um. Yellow boxes indicate regions of magnified overlays on bottom (scale bar = 3um). Plots show quantitation of the manders coefficient (B) for percent of FAs overlapped by α-actinin signal and total α-actinin signal within FAs (C). The respective β1-knockdown cells plated on FN and cFN are shown as orange or blue-checkered boxes. Negative controls include the FAK inhibitor PF-28 (grey) and F-actin destabilizer cytochalasin D (CytoD, brown), both administered to cells on FN. Quantitation of FA lifespan (D) and FA displacement rate (E) are shown from TIRF confocal microscopy videos of HFFs transfected with RFP paxillin (n = 14 cells per substrate). Error bars B-E = min/max. Sparsely-plated HFFs were permitted to randomly migrate over 20 hours, and the resultant computed individual average

cell velocities (F) and persistence distances (G), along with sample fields of view (H) with color lines overlaid to show individual cell displacements demonstrates significant enhancements of both parameters on cFN. Wound healing assays were also performed with resultant contrast-enhanced and binarized images of wound defects are shown in (I) where black = cell coverage and white = underlying matrix. Quantification of percent cell coverage within wound defects is shown in (J), indicating improved wound closure on cFN. Error bars in A, B, and E = SD.

Figure 6

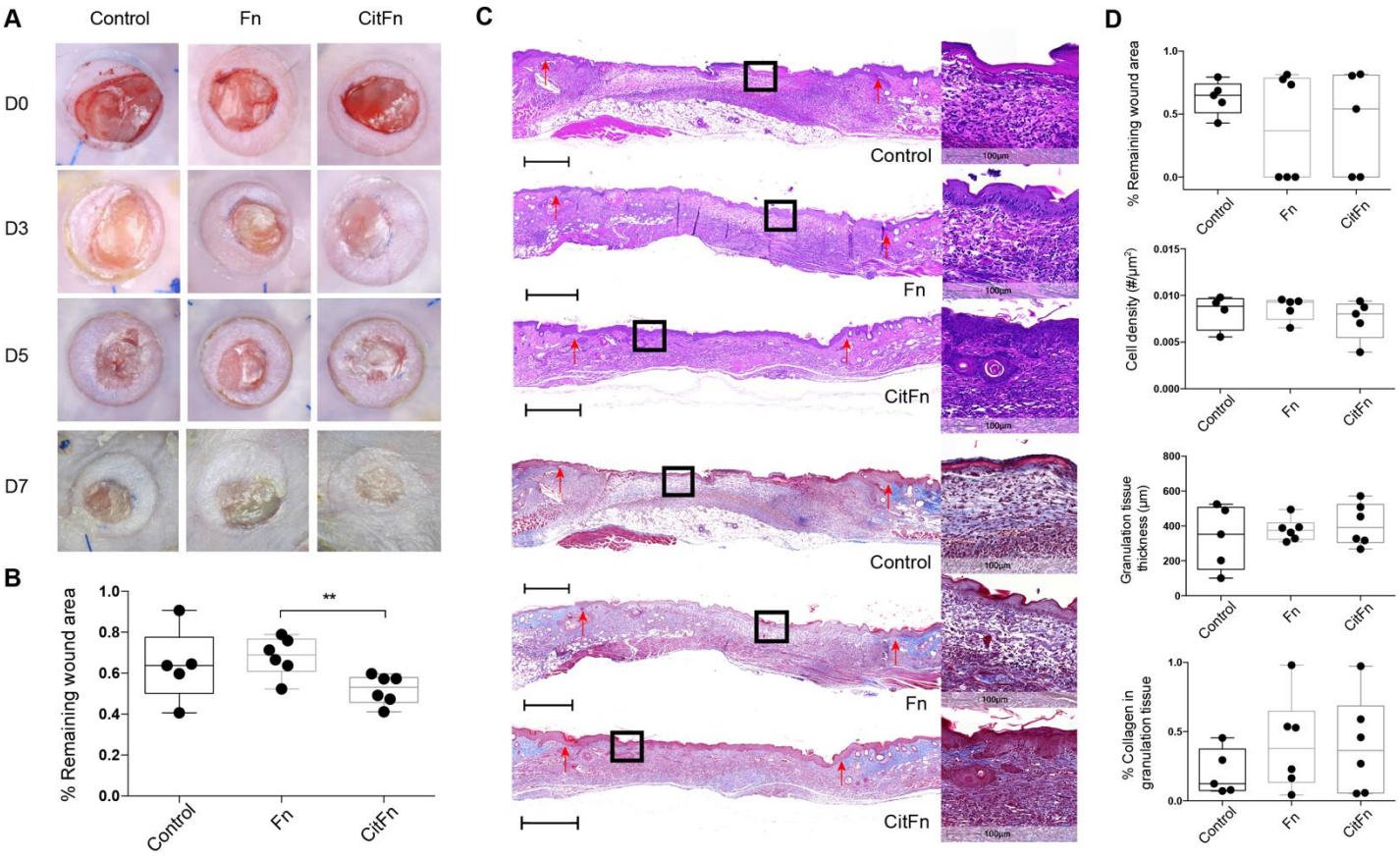

Figure 6 A) Representative images of SKH-1 wound closure at 7 day; B) Quantification of wound closure data from images, statistical significance performed using standard two-tailed t-test between Cit and non-Cit conditions ($P < 0.01$ **) C) Representative H&E and Trichrome staining, from top to bottom: control (fibrin gel), FN, and CitFN, red arrows indicate the edge of the wound, scale bar = 500 μm; D) From top to bottom: remaining wound area quantification from H&E staining; cell density quantification from H&E staining; granulation tissue thickness quantification from Trichrome staining; and collagen percentage quantification from Trichrome staining.

Figure 7

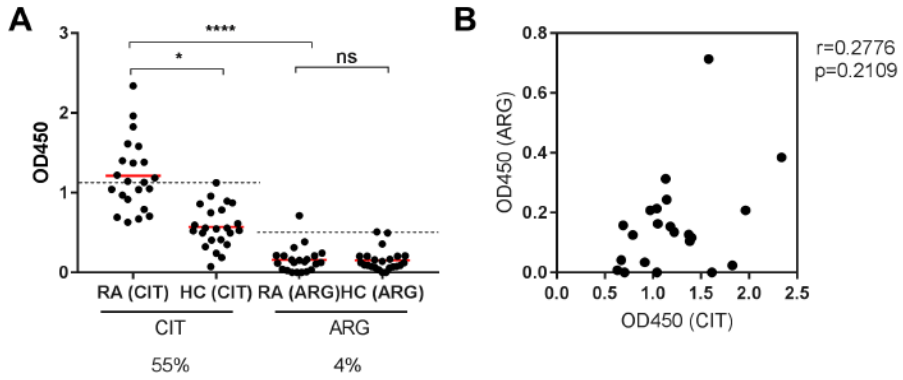

Figure 7. Citrulline specific antibody responses towards a peptide from fibronectin. **(A)** IgG response to the citrullinated fibronectin peptide citFN1410 and the arginine containing control peptide in patients with rheumatoid arthritis (RA; n = 22) and healthy controls (HC, n = 23). Red line indicates the mean. Dotted lines indicate the cut-off level for antibody positivity (98% percentile of healthy control sera). Numbers below graph indicate percentage positivity. Kruskal Wallis test with Dunn's multiple comparison test was used to calculate p-values for differences between groups. **(B)** Spearman-correlation between OD450 Arginine peptide vs OD450 Citrulline peptide in RA sera. ns=no significant difference, *p<0.05 and **p<0.01, ***p<0.001, ****p<0.001). FN - Fibronectin, ARG – arginine peptide, CIT – citrulline peptide.